A98-31566

ICAS-98-3,9,3

LOW SPEED WIND TUNNEL EXPERIMENTS ON A DELTA WING OSCILLATING IN PITCH

D. Hummel
Institute of Fluid Mechanics, Technical University Braunschweig, Germany

T. Loeser
Institute of Design Aerodynamics, DLR Braunschweig, Germany

Abstract

Subject of the present paper are force and pressure measurements performed on a sharp-edged cropped delta wing with 65° leading-edge sweep. Motivation for the tests were the provision of experimental data for validation of unsteady computational codes and understandig of the flow past an oscillating delta wing. The tests were conducted in the Low-Speed Wind Tunnel (NWB) of DNW and included static measurements as well as dynamic measurements with the model oscillating in pitch.

Results of the balance measurements are presented for different sting configurations in static case and for various mean angles of attack in dynamic case.

Results of the pressure measurements are presented for static angles of attack and for pitching oscillations about the mean angles of attack $\alpha_0 = 9°$, $\alpha_0 = 27°$ and $\alpha_0 = 42°$. The corresponding expected flowfields are vortical flow without breakdown, vortical flow with breakdown and vortical flow with breakdown changing to deadwater type flow. Finally, a result of an unsteady Navier-Stokes calculation by W. Fritz is compared with the corresponding experimental result.

1. Introduction

The flow past a delta wing with sharp leading edges differs significantly from the flow past a conventional wing. Even at small angles of attack the flow separates at the leading edges, forming spiral vortices, which lead to a nonlinear increase of lift. At higher angles of attack the phenomenon of vortex breakdown leads to a decline of the lift curve. When the location of the vortex breakdown, which moves forward with increasing angle of attack, reaches the apex, the vortices disappear and a deadwater type flow establishes.

This type of flow has been subject of investigations for many years, e.g. Wilson, Lovell[1], Brown, Michael[2], Peckham[3], Elle[4] and can be considered to be well understood. General discussion of this subject can be found in Hummel[5], [6], Parker[7] and Lee, Ho[8].

The rapid performance increase of computers in the last decades made the development of computational fluid dynamics possible. For the validation of computational codes well documented wind tunnel experiments for rather simple model geometries are essential. The need of such data for delta wings led to the International Vortex Flow Experiment for Computer Code Validation (VFE)[9], [10] in the mid eighties. The majority of the experiments performed in these investigations are concerned with a configuration of a delta wing having a leading edge sweep of 65°, with and without canard, covering a wide range of Mach numbers[11], [12]. Corresponding computational results can be found in Wagner et al.[13], Williams et al.[14], van den Berg et al.[15] and Borsi et al.[16].

The flight envelope of modern fighter aircraft includes rapid, complex maneuvers, sometimes exceeding the angle of attack of maximum lift. In case of a pitch-up motion the maximum dynamic lift of a delta wing exceeds the maximum static lift because of the delay of vortex breakdown movement towards the apex, see Cunningham, den Boer[17], Atta[18] and Soltani et al.[19].

For a prediction of this dynamic behaviour unsteady computational codes had to be developed. Examples of unsteady computational results can be found in Ekaterinaris, Schiff[20], Kandil, Chuang[21], Gordnier, Visbal[22], Chaderjian[23] and Visbal[24].

Suitable unsteady experiments for code validation are less numerous than steady tests. Surveys of unsteady delta wing experiments can be found in Parker[7], Lee, Ho[8], Nelson[25], Ashley et al.[26] and Greenwell, Wood[27]. A compendium of unsteady aerodynamic measurements suitable for code validation, although not including delta configurations, can be found in [28]. The tests described in this paper have been carried out in order to provide new low-speed measurements for comparison with unsteady computational codes and to understand the flowfield around a slender wing oscillating in different modes. When the model geometry for these tests was selected, the VFE configuration was chosen because of the large amount of available static computational and experimental data.

2. Notations

A	Aspect ratio ($A = b^2/s$)
C_D, C_L, C_m	Drag, lift, pitching moment coefficients (based on q_∞, S, c_i, reference point: see Fig. 1, nose-up positive)
C_p	Static pressure coefficient ($C_p = (p-p_\infty)/q_\infty$))
M_∞	Free stream Mach number
Re_∞	Free stream Reynolds number ($Re_\infty = V_\infty \cdot c_i/\nu$)
S	Wing area
V_∞	Free stream velocity
$b = 2s$	Wing span
c_i	Root chord
c_t	Tip chord
d	Fuselage diameter
f_0	Model oscillation frequency
q_∞	Dynamic pressure
m_i	Amplitude of the *i*th harmonic
$s_1(x)$	Local half span
t	Time
x, y, z	Rectangular wing fixed coordinates, origin at wing apex, see Fig. 1
$\alpha(t)$	(instantaneous) angle of attack
α_0	Mean angle of attack
$\Delta\alpha$	Oscillation amplitude
β	Angle of sideslip
λ	Taper ratio ($\lambda = c_t/c_i$)
φ_i	Phase angle of the *i*th harmonic with respect to the model motion
$\varphi(t)$	Instantaneous position within one complete oscillation ($\varphi(t) = \omega \cdot t \cdot \pi/180$)
ν	Kinematic viscosity
ξ, η, ζ	Dimensionless wing-fixed coordinates ($\xi = x/c_i$, $\eta = y/s_1$, $\zeta = z/s_1$)
ω	Radian frequency
ω^*	Reduced frequency ($\omega^* = 2\pi \cdot f_0 \cdot c_i/V_\infty$)

3. Experimental investigations

The measurements have been carried out in the $2.85 * 3.25\ m^2$ Low-Speed Wind Tunnel (NWB) of DNW located at the DLR Braunschweig. The open test section has been used.

3.1 Wind tunnel model

The model used in the wind tunnel tests is the original configuration of the Vortex Flow Experiment[9], [10] according to Fig. 1. The wing consists of a cropped delta wing with a leading-edge sweep of 65°, an aspect ratio A = 1.38 and a taper ratio $\lambda = 0.15$.

Concerning the airfoil in the region between 40% and 75% local chord the NACA 65 A 005 contour was chosen, followed by a straight line to meet the sharp trailing edge with radius $r/c_i = 0.2 * 10^{-3}$. The front part of the airfoil consists of a circular arc which is joined to the NACA 65 A 005 airfoil contour at the point of maximum thickness with horizontal tangent and that meets the sharp leading edge with radius $r/c_i = 0.2 * 10^{-3}$.

The fuselage below the wing has a diameter of $d/c_i = 0.133$. The model is made from carbon fibre composite. Its dimensions

Inner chord c_i = 1200 mm
Span b = 951 mm

are exactly twice the size of the model built earlier by NLR, which has been described in more detail by Hirdes[11].

3.2 Excitation system

For the static and dynamic measurements the model was attached to the Mobile Oscillatory Derivative Balance MOD by means of a belly sting. Static force and moment measurements have been performed with the model being supported by the belly sting without and with rear sting dummy as well as with the model being supported by a rear sting without and with belly sting dummy.

Concerning dynamic tests the mechanical MOD-system is capable of exciting a model in four different modes of forced oscillations, the modes being pitch, roll, yaw and heave. Measurements have been carried out for pitch, roll and yaw[29]. In the present context only the pitching motion will be treated, which took place about an axis in spanwise direction at

$x/c_i = 0.5625$ and $z/c_i = -0.042$.

The centre of motion was located on the fuselage centre-line. The maximum oscillation frequency f_0 of the MOD is 3.0 Hz and the largest possible oscillation amplitudes for the pitching motion are $\Delta\alpha = 10°$.

The mechanical MOD-system is equipped with a deflection sensor which indicates the instantaneous position of the model. For the data acquisition the Transputer Expandable Data Acquisition System TEDAS has been used. Its maximum sampling frequency per channel is 50 kHz.

3.3 Instrumentation

3.3.1 Balance measurements

Forces and moments have been measured by means of an internal six-component strain-gauge balance of type Emmen-196-6[29]. In the evaluation of the aerodynamic coefficients the pitching moment reference point was chosen in the symmetry plane of the wing $z/c_i = 0$ at $x/c_i = 0.5625$. Therefore, the pitching moment reference point does not coincide with the centre of the pitching oscillation.

Since the balance measurements always comprise of both the aerodynamic and the inertial forces and moments, a set of experiments without the external flow, $V_\infty = 0$, has been carried out in order to determine the contribution of the inertia forces and moments. The results of these experiments have been subtracted from the results of the measurements with free stream flow V_∞ in order to get the aerodynamic forces and moments separately.

The data acquisition of the balance signals has been carried out by means of the TEDAS system.

3.3.2 Pressure measurements

The model is equipped with 230 pressure taps which are located in three sections $x/c_i = 0.3$, 0.6 and 0.8. Their positions may be taken from Fig. 1 (see also Loeser[29]). All taps have been connected to modules of the PSI pressure measurement system and through the main PSI data acquisition unit a sampling frequency of 72 Hz has been achieved.

In addition to the PSI pressure measurement system 9 Kulite pressure transducers of the types XCS-062 and XCS-093 have been installed in the model. The locations of these Kulites may be taken from Fig. 1. They are connected to the same pressure taps as the corresponding PSI connectors via Y-shaped manifolds. Concerning the data acquisition of the signals from the Kulites the TEDAS system has been used. The PSI-system and the TEDAS system were synchronized, and the Kulite measurements were used to check the two systems with respect to pressures and synchronisation.

3.4 Data evaluation

After the elimination of the inertial forces from the balance data, as described in section 3.3.1, the data from force and pressure measurements are treated identically. After conversion to dimensionless coefficients, the data have been transformed into the frequency domain via Fourier transformation. It was found that the first three harmonics of the oscillation frequency are sufficient to reproduce the original data. Phases φ_i of the three harmonics with respect to the position signal and amplitudes m_i were calculated from real and imaginary parts according to the following relations:

$$m_i = \sqrt{Re_i^2 + Im_i^2}$$

and

$$\tan\varphi_i = -Im_i / Re_i .$$

The index i stands for the *i*th harmonic. With this definition of the phase angles, positive values stand for force or pressure coefficients leading the model motion. The signals f in the time domain can now be written as

$$f(t) = m_0 + \sum_{i=1}^{3} m_i \cdot \cos(i\omega t + \varphi_i) ,$$

m_0 being the constant offset stemming from the Fourier transformation[30].

Because every measurement with a certain parameter combination has been repeated up to six times, a statistical analysis could be performed on the outcome of the Fourier transformation. Values, which appeared to be significantly out of line, were rejected according to Chauvenet's criterion, see Coleman, Steele[31] for details.

Finally, the remaining data were fed into an analysis of variance (ANOVA), a statistical technique suitable for evaluating the quantitative and qualitative effects of one or more experimental factors (Reynolds number, oscillation frequency, oscillation amplitude) on a response variable (any of the amplitudes and phases of a certain pressure tap or force coefficient at a fixed angle of attack). Among the results of the ANOVA are

- the statistical significance of an experimental factor on the response variable, and
- the amount of variation, which cannot be assigned to changes in experimental factors and from which confidence intervals for the response variable can be calculated.

For more details concerning the ANOVA see Mason et al.[32], Johnson, Leone[33] and Storm[34]. The complete results of the ANOVA applied on the experiment described in this paper can be found in Loeser[29]. A typical result of the analysis of variance is shown in Fig. 2. For the pressure distribution in the section $\xi = 0.6$ the amplitudes and phases of pitching motions with $\alpha_0 = 9^\circ$ and $Re_\infty = 3.1*10^6$ are shown for two different amplitudes $\Delta\alpha$ and two different reduced frequencies ω^*. The error bars indicate the range for an uncertainty of 5%.

3.5 Scope of measurements

The wind tunnel measurements have been carried out for freestream velocities $V_\infty = 20$ m/s and 40 m/s, corresponding to Reynolds numbers $Re_\infty = V_\infty \cdot c_i/\nu = 1.55 * 10^6$ and $3.10 * 10^6$ and Mach numbers $M_\infty = 0.06$ and $M_\infty = 0.12$. All measurements have been performed in symmetrical flow ($\beta = 0^\circ$). The excitation frequencies used in the tests were $f_0 = 1.5$ Hz and 3.0 Hz. The combination with the two free stream velocities led to reduced frequencies of $\omega^* = 2\pi \cdot f_0 \cdot c_i/V_\infty =$

0.28 and 0.56 for $Re_\infty = 3.1 * 10^6$ and
0.56 and 1.12 for $Re_\infty = 1.55 * 10^6$.

The wind tunnel tests have been performed for certain combinations of the mean angle of attack α_0 and the oscillation amplitude $\Delta\alpha$, as indicated in Tab. 1. Their choice is closely related to the expected flow types:

$\alpha_0 = 0^\circ$: In this case the vortex formation will alternate between the upper and the lower surface of the configuration during the pitching motion.

$\alpha_0 = 9^\circ$: Vortices will be present over the upper surface of the configuration and no vortex breakdown will occur during the whole cycle of the pitching motion.

$\alpha_0 = 15^\circ$,

$\alpha_0 = 21^\circ$: These conditions are related to mixed cases without vortex breakdown over the configuration at low angles of attack and with vortex breakdown at high angles of attack during the cycle of motion.

$\alpha_0 = 27^\circ$: Vortices with vortex breakdown are expected to occur over the upper surface of the configuration and this type of flow will be present during the whole cycle of the pitching motion.

$\alpha_0 = 42^\circ$: During the cycle of the pitching motion the flow is expected to switch between a vortex-type flow with vortex breakdown and a dead-water-type flow.

$\alpha_0 = 48^\circ$: In this case a deadwater-type flow is expected during the whole cycle of motion.

The scope of the measurements may be taken from Tab. 1.

4. Results

4.1 Steady flow

The results of the static 3-component balance measurements are shown in Fig. 3. Concerning the different sting configurations no effects were found related to the lift and drag coefficients, but in the presence of a belly sting the pitching moment coefficients are slightly larger than in the case of a rear sting. The difference is due to the higher pressures upstream and the lower pressures downstream of the belly sting which produce an additional nose-up pitching moment. The effects of Reynolds number on the static aerodynamic coefficients is very small, see Loeser[29].

The static pressure distribution in the section at $\xi = 0.6$ is given in Fig. 4 for different values of the angle of attack. At $\alpha = 0^\circ$ the well-known pattern without vortices turns out and with increasing angle of attack the suction peaks underneath the vortices increase in magnitude. For $\alpha > 24^\circ$ vortex breakdown occurs upstream of the section under consideration and correspondingly the magnitude of the suction peaks decreases with further increasing angle of attack. The high suction peaks in the region of the primary vortex and the considerably lower suction peaks in the region of the secondary vortex indicate that the upper surface boundary layer is turbulent at the Reynolds number $Re = 3.1 * 10^6$ under consideration.

The static pressure distribution is again plotted in Fig. 5 for all three sections $\xi = 0.3$, $\xi = 0.6$ and $\xi = 0.8$ as a function of the angle of attack. Lines of constant pressure coefficient C_p are shown. In all three sections the vortex-type flow is indicated by the suction peaks which increase with increasing angle of attack. If vortex breakdown occurs the peaks are reduced and the region of suction is broadened in spanwise direction. Vortex breakdown crosses the sections

$x/c_i = 0.8$ at $\alpha = 20^\circ$
$x/c_i = 0.6$ at $\alpha = 24^\circ$
$x/c_i = 0.3$ at $\alpha = 29^\circ$.

For larger angles of attack the flow with vortex breakdown is still marked by a nonuniform pressure distribution against span. At $\alpha = 43^\circ$ the vortex breakdown position reaches the apex of the configuration. The vortex-type flow suddenly dissappears. The deadwater-type flow in the centre of the vortex with vortex breakdown is no longer surrounded by an ordinary vortex flow. The deadwater-type flow establishes over the whole upper surface of the configuration simultaneously and the static pressure becomes constant everywhere on the upper surface.

4.2 Unsteady flow

4.2.1 Balance measurements

The results of the unsteady 3-component balance measurements of pitching oscillations about different mean angles of attack at $Re_\infty = 3.10 * 10^6$ with an amplitude of $\Delta\alpha = 6.0^\circ$ and a reduced frequency of $\omega^* = 0.56$ are shown in Fig. 6. The arrows indicate the direction of the hysteresis loops. Lift as well as drag reach higher values during the upstoke part of the oscillation cycle. At small to medium mean angles of attack the hysteresis loops of lift and drag follow the static curve closely.

The instantaneous local angle of attack at any point of the model depends on the distance from the oscillation axis. During the upstroke part of the oscillation cycle this local angle of attack is higher on that part of the model, which is located behind the oscillation axis. Therefore, the contribution to the lift from the rear part of the wing is higher during the upstroke part and leads to a lower (more nose-down) pitching moment.

At large mean angles of attack ($\alpha_0 = 42.0^\circ$ and $\alpha_0 = 48.0^\circ$) the dynamic curves deviate strongly from the corresponding static values. At $\alpha_0 = 42.0^\circ$ the dynamic lift doesn't show the sudden drop indicating the change from vortical to deadwater type flow. The almost constant value for the lift indicates a persistence of vortical flow during the whole oscillation cycle. At $\alpha_0 = 48.0^\circ$ in the dynamic case the deadwater type flow is present during the complete oscillation cycle, whereas in the steady case the flow changes from deadwater to vortical type and vice versa.

4.2.2 Pressure measurements

Some results of the dynamic pressure distribution measurements are shown in Figs 7 to 9. Lines $C_p = \text{const.}$ are shown for the section $\xi = 0.6$ for one complete oscillation cycle, starting from the mean angle of attack in upstroke direction. The figures on the left show the results for a quasi-steady oscillation ($\omega^* = 0$), and the figures on the right depict oscillations with a reduced frequency of $\omega^* = 0.56$. The oscillation amplitude is $\Delta\alpha = 6.0^\circ$ and the Reynolds number is $Re_\infty = 3.1 * 10^6$ for all figures.

Since the wind tunnel tests indicated that in the static case the pressure distributions are independent of the α history, the quasistatic figures have been calculated from measurements taken at increasing angle of attack only, which results in exact symmetry of the iso-C_p-lines with respect to $\varphi = 90^\circ$ and $\varphi = 270^\circ$. The dynamic pressure distributions have been calculated from the first three harmonics, which are the outcome of the data evaluation described in section 3.4.

Fig. 7 shows pressure distributions for $\alpha_0 = 9.0^\circ$. In the quasi-steady as well as in the dynamic case vortical flow without breakdown exists during most of the cycle. In the vicinity of $\alpha = 3^\circ$ the vortices disappear and attached flow establishes in both cases. The spanwise

position of the vortex, indicated by the position of the suction peak and emphasized in Fig. 7 with bold lines, moves inward with increasing angle of attack in both cases. In the dynamic case the spanwise position of the re-establishing vortex is located closer to the leading edge and the suction peak reaches its peak value before the maximum angle of attack is reached.

The quasistatic and dynamic pressure distributions at $\alpha_0 = 27.0^o$ are shown in Fig. 8. In the quasistatic case no vortex breakdown takes place in the section $\xi = 0.6$ for $\alpha < 24^o$, corresponding to $210^o \le \varphi \le 330^o$. For the rest of the cycle vortex breakdown affects the pressure distribution in the section $\xi = 0.6$, resulting in a less narrow suction peak, as indicated by the bigger spacing of the iso-C_p-lines in spanwise direction.

Laser light sheet measurements, which have been performed on the static and oscillating model revealed that, compared to the static case, the mean position of vortex breakdown is located further upstream and that the movement of the breakdown location with the angle of attack is reduced in the dynamic case. Vortex breakdown is located in front of the section $\xi = 0.6$ during the complete cycle. This results in a single suction peak maximum, which is of smaller magnitude than in the static case. The suction peak does not reach its peak value at minimum angle of attack ($\varphi = 270^o$) but at $\varphi = 345^o$ because of the delay of the breakdown position with respect to the model deflection.

At a mean angle of attack of $\alpha_0 = 42.0^o$ quasistatic and dynamic pressure distributions vary considerably, as can be seen in Fig 9. As already stated in section 4.2.1, the flow changes from a vortical type to a deadwater type with constant pressure coefficient in spanwise as well as in longitudinal direction. This is true for the quasistatic case, depicted on the left side of Fig 9. In the dynamic case vortex breakdown does not reach the apex and therefore vortical flow persists. As with $\alpha_0 = 27.0^o$ position and magnitude of the suction peak can be explained by the mean position and the delay of the breakdown position with respect to the model deflection.

5. Comparison with numerical results

Euler and Navier-Stokes calculations of pitching oscillations with $\alpha_0 = 9.0^o$, $Re_\infty = 3.1 * 10^6$ and $\omega^* = 0.56$ have been performed by W. Fritz[35]. The geometry used was identical with the model described above except for a slightly different wingtip configuration and the absence of the fuselage. The Mach number has been raised to $M = 0.4$ in order to reduce computation time.

Fig 10 shows pressure distributions at $\xi = 0.6$ resulting from the Navier-Stokes computation and from the wind tunnel tests. Generally, the agreement is very good, the lateral movement of the primary vortex axis is reproduced excellently. The figures with the pressure distributions at $\alpha = 9.0^o$ in upstroke and downstroke directions contain also static pressure distributions for comparison. In the experiment as well as in the calculation the suction peak is higher in the upstroke motion in comparison with the static case and lower in the downstroke motion in comparison with the static case. A Fourier analysis performed on the calculated pressure distributions indicated that the differences in the heights of the suction peaks noticeable at $\alpha = 6.0^o$ and $\alpha = 12.0^o$ can be related to a larger phase lead of the first harmonic in the calculation.

Conclusions

Wind tunnel tests have been performed on a delta wing having the geometry of the Vortex Flow Experiment. The aim was to provide experimental results for comparison with unsteady computational results and to understand the flowfield around the moving model.

6-component balance measurements as well as pressure measurements have been carried out with the model in fixed position and oscillating in pitch. Investigations on different sting configurations in the static case revealed very little influence.

For the description of the dynamic forces and pressures the first three harmonics of the model oscillation frequency have been found to be sufficient. The effects of the experimental parameters, such as reduced frequency, oscillation amplitude and Reynolds number, on the amplitudes and phases of the first three harmonics have been specified qualitatively and quantitatively by means of an analysis of variance. This statistical method also provides confidence intervals for the amplitudes and phases of the harmonics.

Although the influence of vortex breakdown on the dynamic forces is small, differences between quasistatic and dynamic pressure distributions become large in the presence of vortex breakdown. At very high angles of attack the type of flow remains the same during the oscillation in the dynamic case (either vortical or deadwater type flow), whereas the flow type changes in the quasistatic case.

As a first testcase for numerical code validation an oscillation with $\alpha_0 = 9.0^o$ and $\Delta\alpha = 3^o$, the flowfield being of vortical type without breakdown during the complete cycle, is recommended. A Navier-Stokes calculation for this case has been performed by W. Fritz[35], the agreement between calculation and experiment is very good.

References

[1] Wilson Jr., H.A., Lovell, J.C.: Full scale investigation of the maximum lift and flow characteristics of an airplane having approximately triangular planform. NACA RM L6K20 (1947)

[2] Brown, C. E., Michael, W. H.: Effects of leading-edge separation on the lift of a delta wing. J. Aeron. Sci 21 (1954), pp. 690 - 694

[3] Peckham, D. H.: Low-speed wind-tunnel tests on a series of uncambered slender pointed wings with sharp edges. ARC Rep. Mem. 3186 (1958)

[4] Elle, B. J.: On the breakdown at high incidences of the leading edge vortices on delta wings. J. Roy. Aeron. Soc. 64 (1960), pp. 491 - 493

[5] Hummel, D.: On the vortex formation over a slender wing at large angles of incidence. AGARD-CP-247 (1978), pp. 15-1 to 15-17

[6] Hummel, D.: Documentation of separated flows for computational fluid dynamics validation. AGARD-CP-437 (1988) Vol. 2, pp. P15-1 to P15-24

[7] Parker, A. G.: Aerodynamic characteristics of slender wings with sharp leading edges - a review. J. Aircraft 13 No. 3 (1976), pp. 161 - 168

[8] Lee, M., Ho, C.-M.: Vortex dynamics of delta wings. In: Gad-el-Hak, M. (Ed.): Frontiers in Experimental Fluid Mechanics. Lecture Notes in Engineering, Vol. 46, Springer Verlag, Berlin, 1989, pp. 365 - 427

[9] Drougge, G.: The international vortex flow experiment for computer code validation. ICAS-Proc. 1988, Vol. 1, pp. XXXV - XLI

[10] Elsenaar, A., Hjelmberg, L., Bütefisch, K., Bannink,W. J.: The International Vortex Flow Experiment. AGARD-CP-437 (1988), Vol. 1 , pp. 9-1 to 9-23

[11] Hirdes, R. H. C. M.: US/European Vortex Flow Experiment test report of wind-tunnel measurements on the 65° wing in the NLR High Speed Wind Tunnel HST. NLR TR 85046 L (1985)

[12] Hummel, D., Oelker, H.-Chr.: Low-speed characteristics for the wing-canard configuration of the International Vortex Flow Experiment. J. Aircraft 31, (1994), pp. 868 - 878

[13] Wagner, B., Hitzel, S. M., Schmatz, M. A., Schwarz, W., Hilgenstock, A., Scherr, S.: Status of CFD validation on the Vortex Flow Experiment. AGARD-CP-437 (1988), Vol. 1 , pp. 10-1 to 10-10

[14] Williams, B. R., Kordulla, W., Borsi, M., Hoeijmakers, H. W. M.: Comparison of solutions of various Euler solvers and one Navier-Stokes-solver for the flow about a sharp-edged cropped delta wing. AGARD-CP-494 (1991), pp. 2-1 to 2-12

[15] Van den Berg, J. I., Hoeijmakers, H. W. M., Jacobs, J. M. J. W.: Analysis of an Euler-equation method applied to leading-edge vortex flow. AGARD-CP-494 (1991), pp. 4-1 to 4-12

[16] Borsi, M., Formaggia, L., Hettena, E., Santillan, S., Selmi, V., Tarditi, S.: Vortical flow simulation by using structured and unstructured grids. AGARD-CP-494 (1991), pp. 3-1 to 3-12

[17] Cunningham Jr., A., den Boer, R.: Steady and unsteady aerodynamics of a pitching straked wing model at high angles of attack. AGARD-CP-494 (1991), pp. 29-1 to 29-12

[18] Atta, R. A.: Unsteady structure of flow past a pitching delta wing. Dissertation, Lehigh Univ., 1987

[19] Soltani, M., Bragg, M., Brandon, J.: Measurements on an oscillating 70-deg delta wing in subsonic flow. J. Aircraft 27, (1990), pp. 211 - 217

[20] Ekaterinaris, J. A., Schiff, L. B.: Navier-Stokes solutions for an oscillating double-delta wing. J. Aircraft 32 (1995), pp. 228 - 234

[21] Kandil, O. A., Chuang, H. A.: Unsteady vortex-dominated flows around maneuvering wings over a wide range of Mach numbers. AIAA-Paper 88-0317, (1988)

[22] Gordnier, R., Visbal, M.: Numerical simulation of delta-wing roll. AIAA-Paper 93-0554 (1993)

[23] Chaderjian, N. M.: Navier-Stokes prediction of large-amplitude delta-wing roll oscillations. J. Aircraft 31 (1994), pp. 1333 - 1340

[24] Visbal, M.: Onset of vortex breakdown above a pitching delta wing. AIAA Journal 32 (1994), pp. 1568 - 1575

[25] Nelson, R. C.: Unsteady aerodynamics of slender wings. AGARD-R-776 (1991), pp. 1-1 to 1-25

[26] Ashley, H., Jarrah, M. A. M., Katz, J., Vaneck, T.: Unsteady aerodynamic loading of delta wings for low and high angles of attack. Proc. Int. Symposium on Nonsteady Fluid Dynamics (1990), pp. 16 - 78

[27] Greenwell, D., Wood, N.: Some observations on the dynamic response to wing motion of the vortex burst phenomenon. Aeron. Journal 98 (1994), pp. 49 - 59

[28] AGARD (Ed.): Compendium of Unsteady Aerodynamic Measurements. AGRD-R-702 (1982)

[29] Loeser, T.: Dynamic force and pressure distribution measurements on an oscillating delta wing at low speeds. DLR-IB 129-96/9 (1996)

[30] Beckwith, T. G., Buck, N. L., Marangoni, R. D.: Mechanical Measurements. 3rd Ed. Addison-Wesley, Reading Massachusetts, 1981

[31] Coleman, H., Steele Jr., W.: Experimentation and Uncertainty Analysis for Engineers. John Wiley & Sons, New York, 1989

[32] Mason, R., Gunst, R., Hess, J.: Statistical Design and Analysis of Experiments. John Wiley & Sons, New York, 1989

[33] Johnson, N. L., Leone, F. C.: Statistics and Experimental Design in Engineering and the Physical Sciences. Vol. II, 2nd Ed. John Wiley & Sons, New York, 1964

[34] Storm, R.: Wahrscheinlichkeitsrechnung, Mathematische Statistik und Qualitätskontrolle. Fachbuchverlag Leipzig, 1995

[35] Fritz, W.: Unsteady Navier-Stokes calculations for a delta wing oscillating in pitch. ICAS-98-2.4.1, Sept. 1998

Mean angle of attack α_0	Oscillation amplitude $\Delta\alpha$	Free stream velocity V_∞	Oscillation frequency f_0	Reduced frequency ω^*	Reynolds number Re_∞
0°	6°			0.28/0.56/1.12	$1.55 * 10^6/3.1 * 10^6$
9°	3°, 6°			0.28/0.56/1.12	$1.55 * 10^6/3.1 * 10^6$
15°	3°, 6°	20 m/s	1.5 Hz	0.28/0.56/(1.12)	$(1.55 * 10^6)/3.1 * 10^6$
21°	(3°), 6°	and	and	0.28/0.56/1.12	$1.55 * 10^6/3.1 * 10^6$
27°	3°, 6°	40 m/s	3.0 Hz	0.28/0.56/1.12	$1.55 * 10^6/3.1 * 10^6$
42°	6°			0.28/0.56/(1.12)	$(1.55 * 10^6)/3.1 * 10^6$
48°	[6°]			[0.28/0.56]	$[3.1 * 10^6]$

Tab. 1: Scope of the balance and pressure distribution measurements, pitching motion
[] balance measurements only
() pressure measurements only

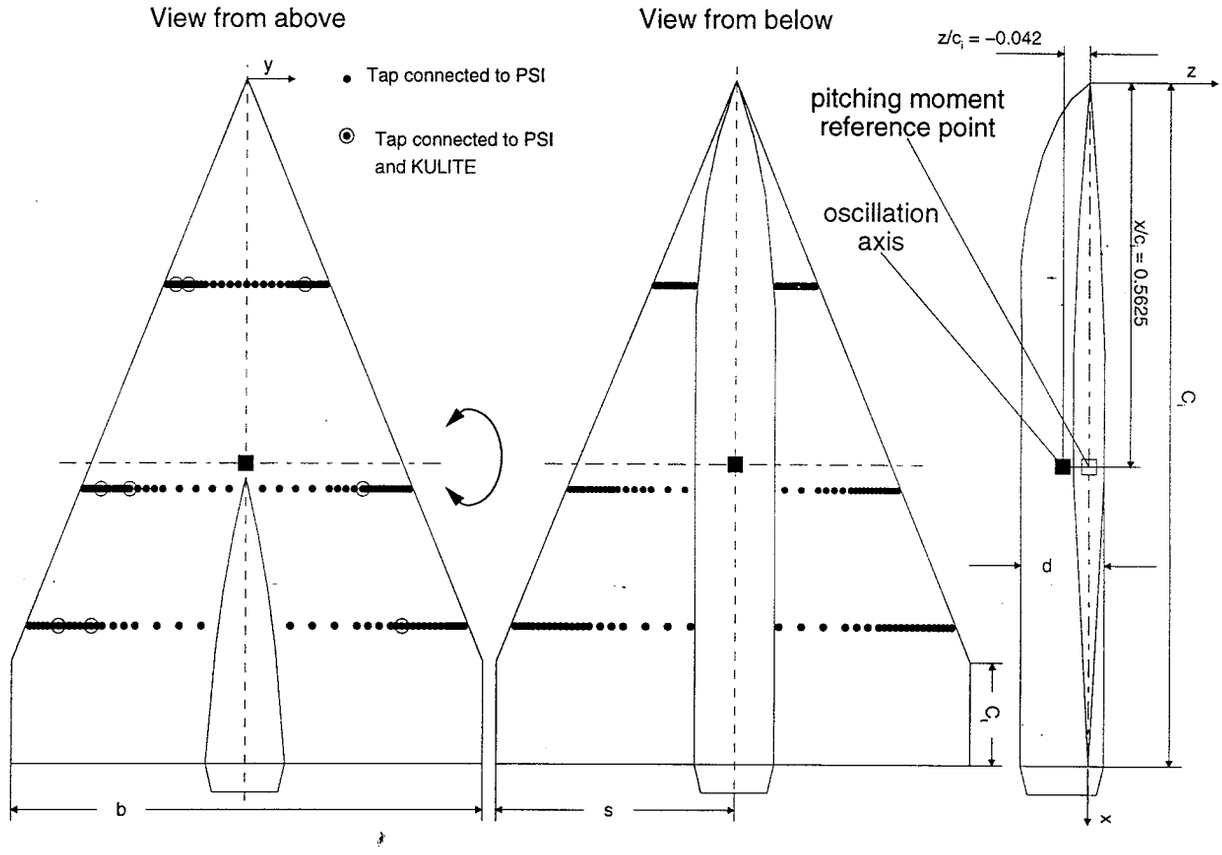

Fig. 1: Wind tunnel model for dynamic balance and pressure distribution measurements

dynamic Loads

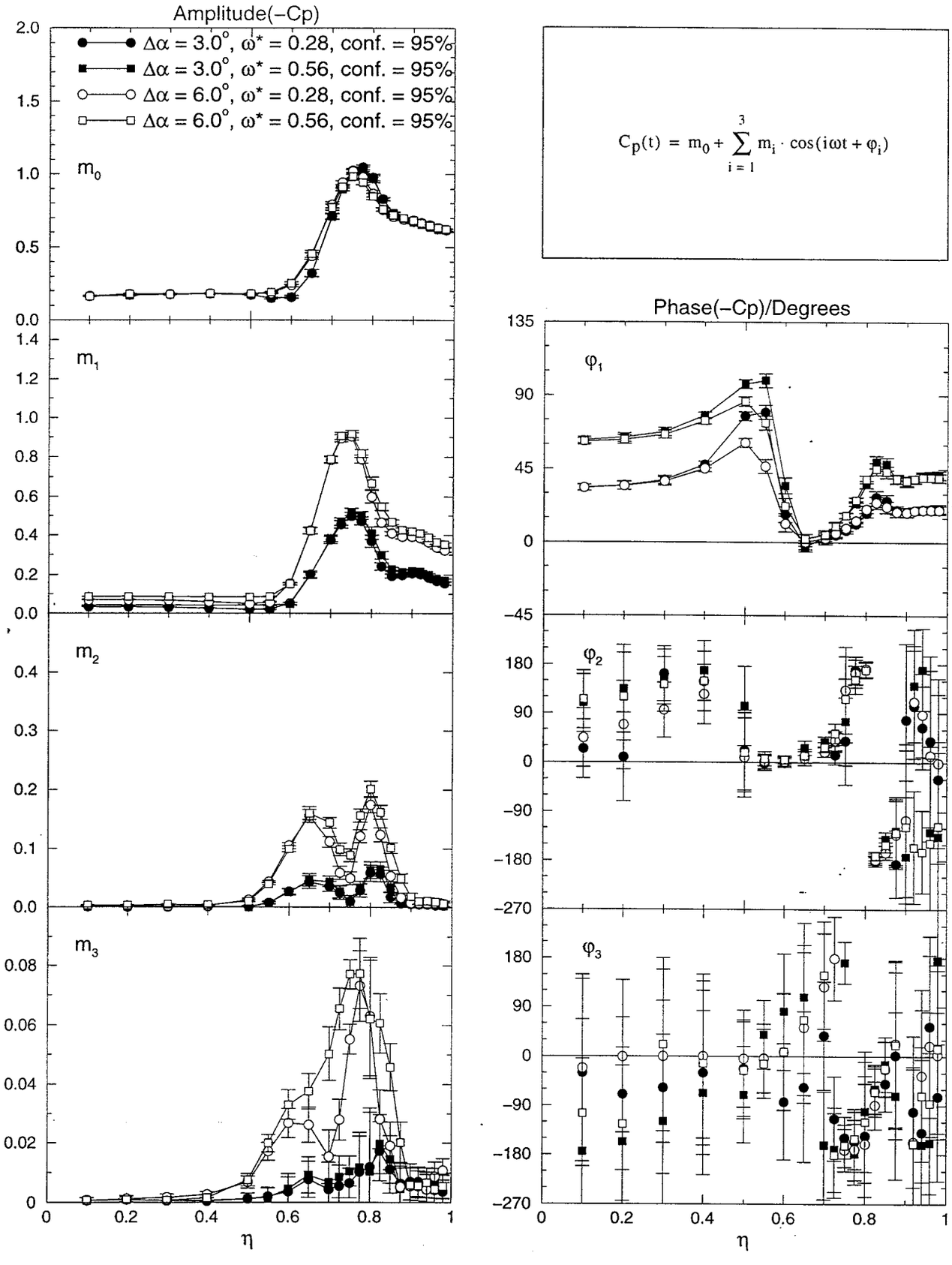

Fig. 2: Typical result of an analysis of variance for the unsteady pressure distribution $C_p(\eta)$ in the section $\xi = 0.6$. Pitching motion with $\alpha_0 = 9^\delta$ and factors $\Delta\alpha$ and ω^* at $Re_\infty = 3.1 * 10^6$, error bars shown for a confidence of 95 %.

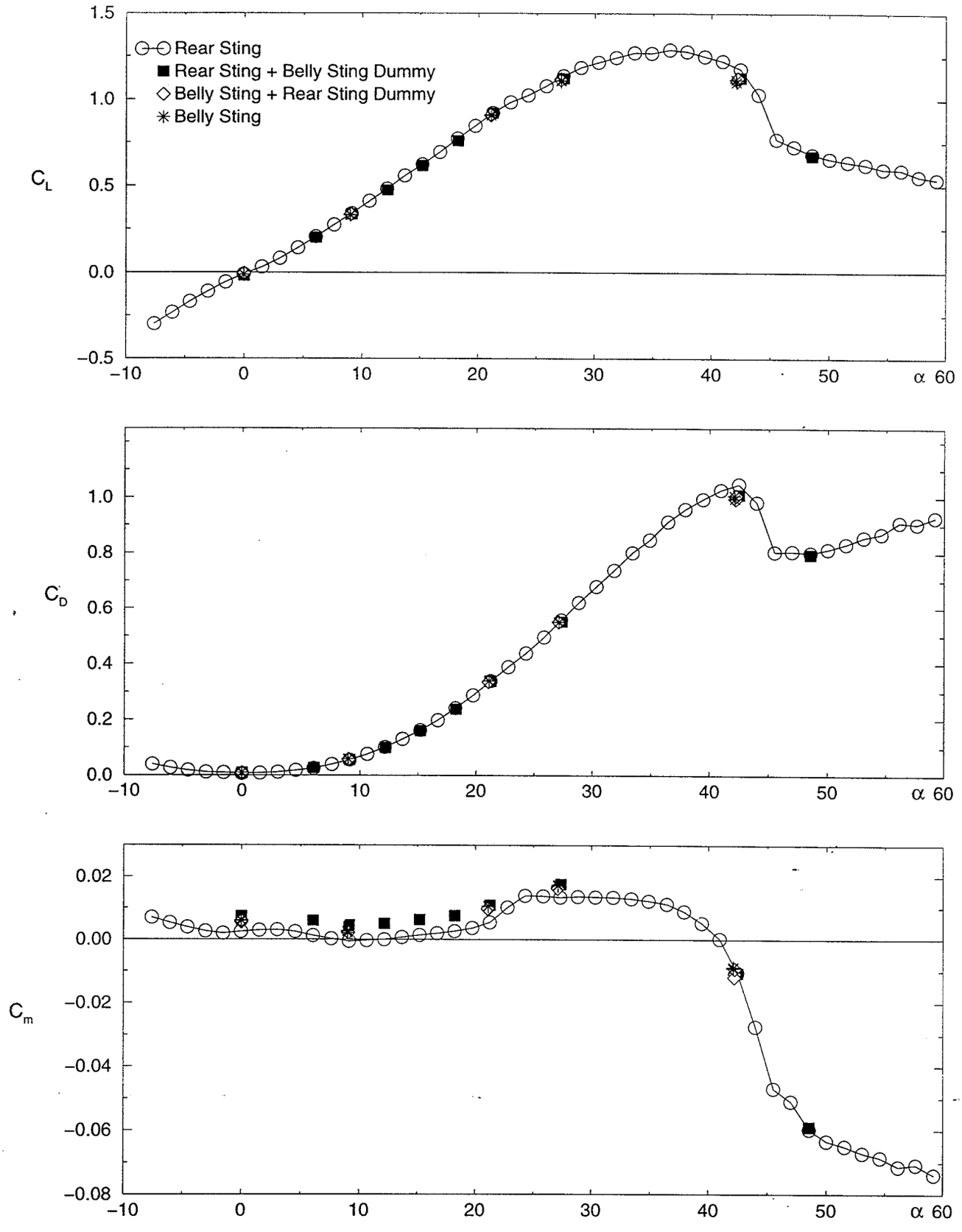

Fig. 3: Results of the static 3-component measurements at $Re_\infty = 3.1 * 10^6$. Effect of different sting configurations.

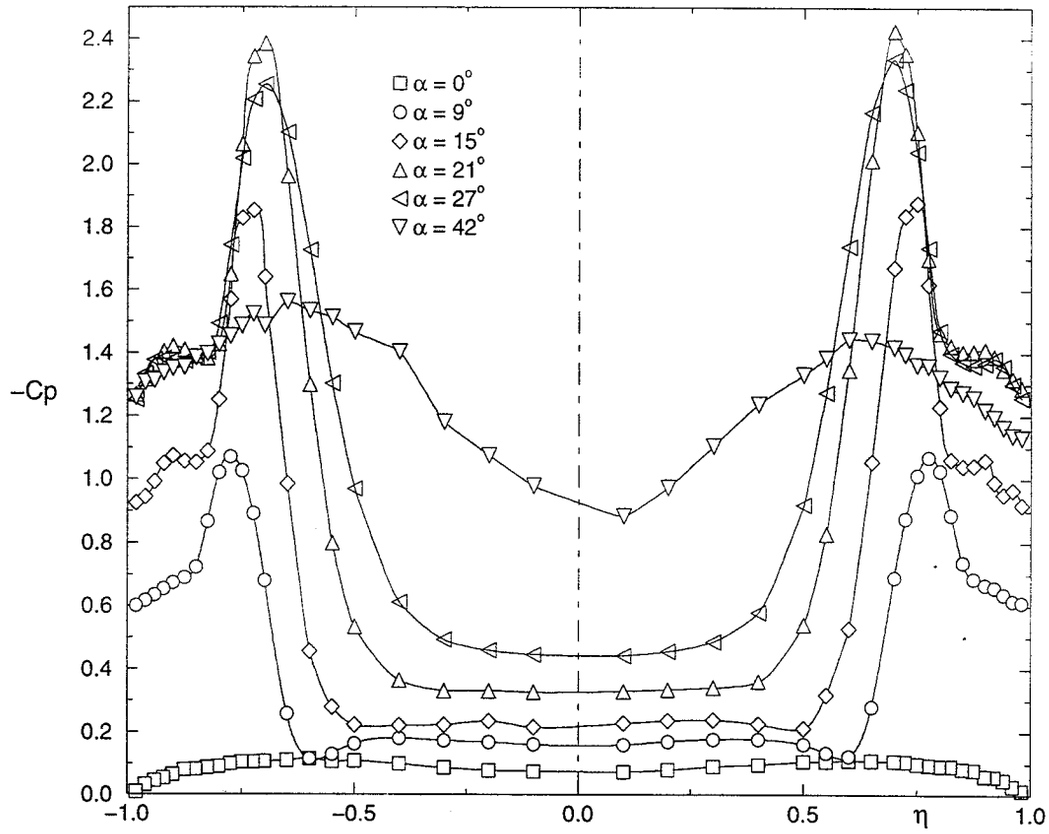

Fig. 4: Static pressure distributions in the section $\xi = 0.6$ for different angles of attack at $Re_\infty = 3.1 * 10^6$.

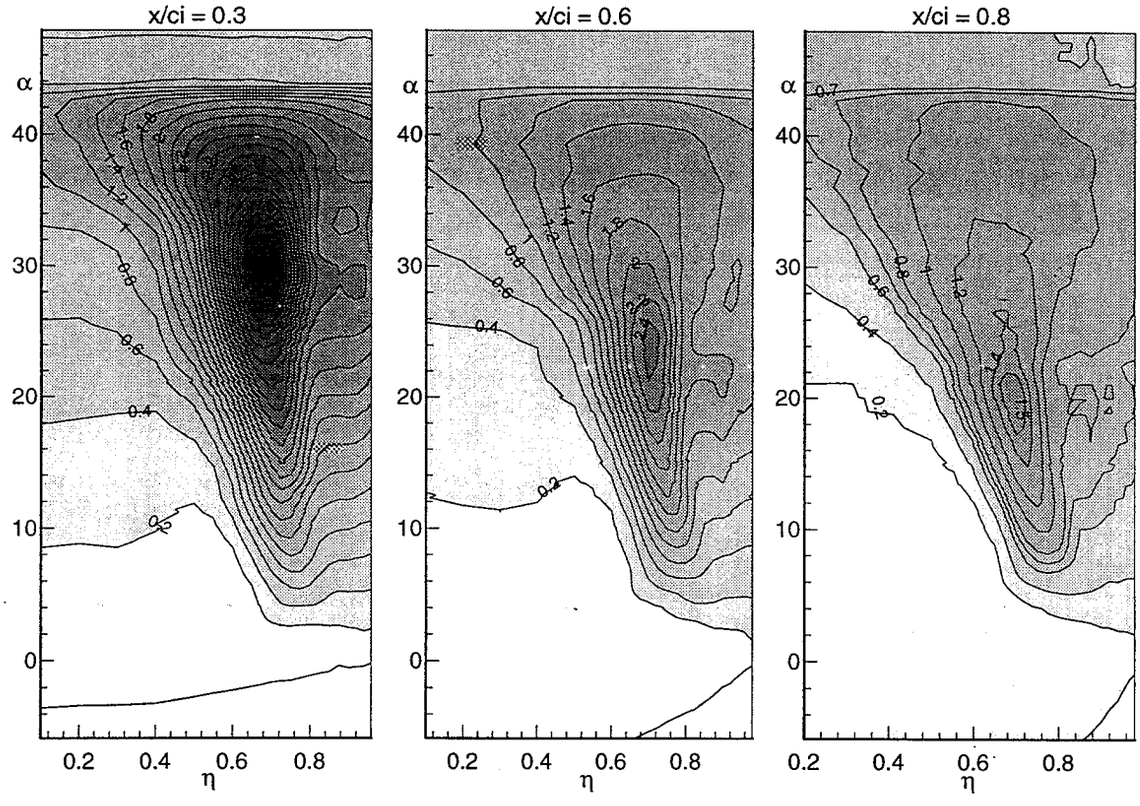

Fig. 5: Static pressure distributions, with lines C_p = const. in the sections $\xi = 0.3$, $\xi = 0.6$ and $\xi = 0.8$ for different angles of attack, $Re_\infty = 3.1 * 10^6$.

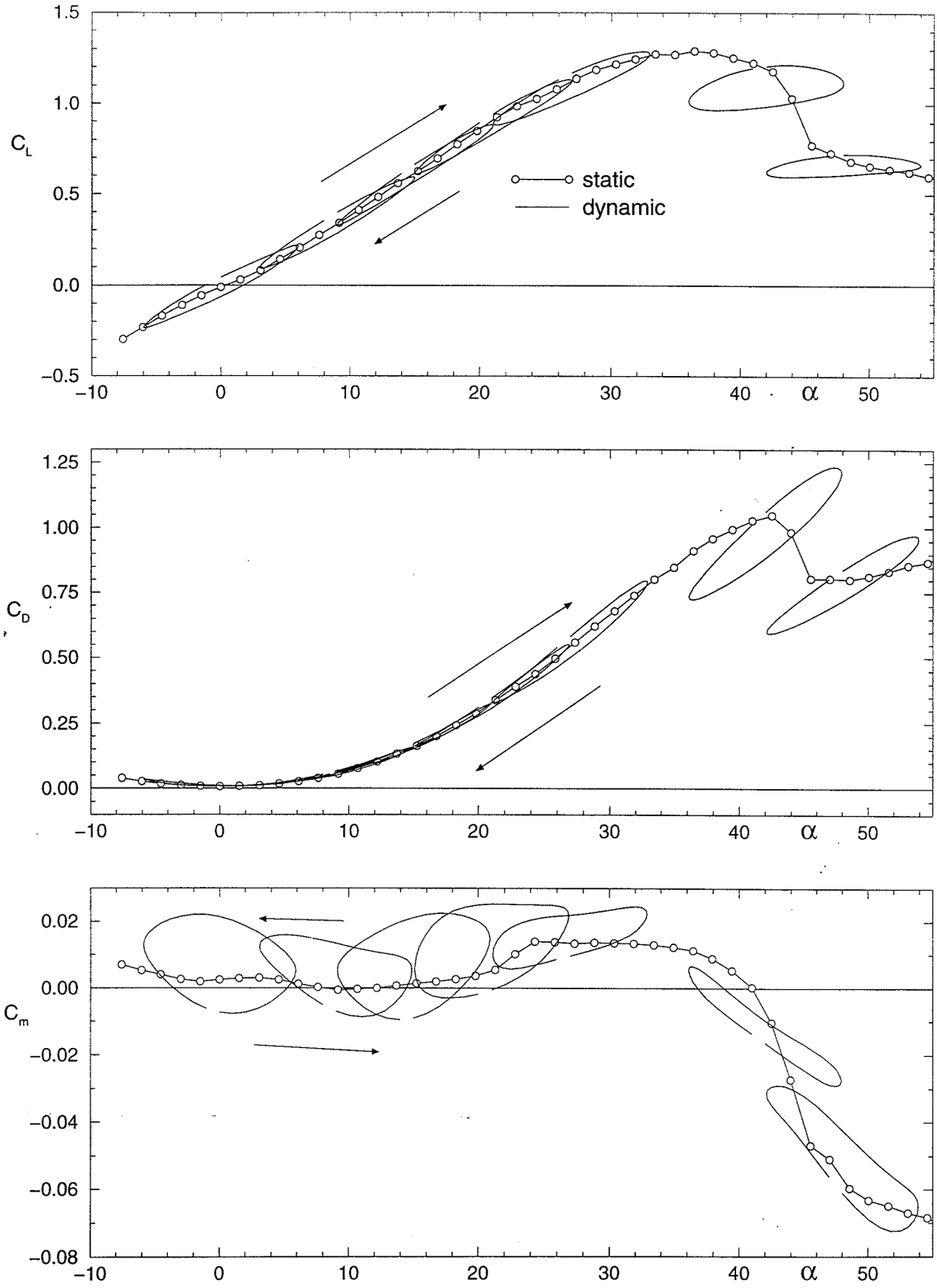

Fig. 6: Static and dynamic results of the 3-component measurements at $Re_\infty = 3.1 * 10^6$. Dynamic parameters: $\omega^* = 0.56$, $\Delta\alpha = 6.0^o$.

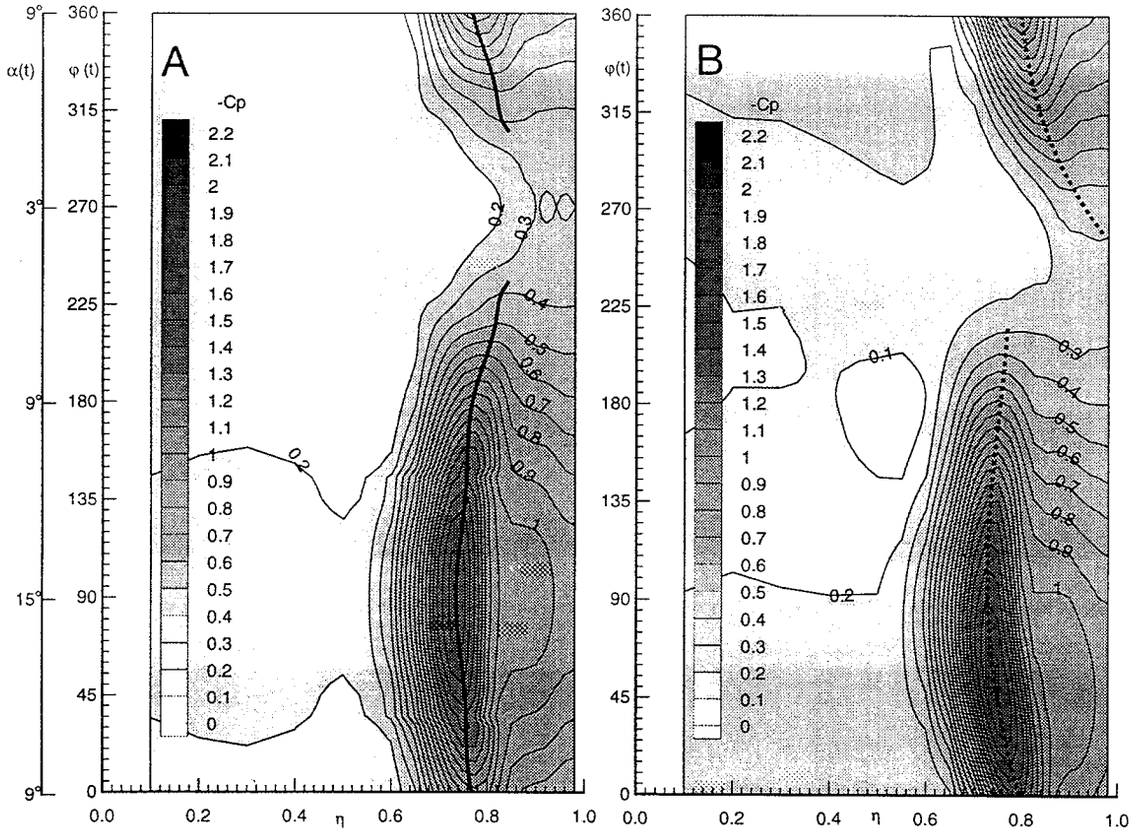

Fig. 7: Quasistatic and dynamic pressure distribution with lines C_p = const. in the section $\xi = 0.6$ for pitching oscillation with $\alpha_0 = 9^o$, $\Delta\alpha = 6^o$, $Re_\infty = 3.1 * 10^6$. A: quasistatic ($\omega^* = 0$), B: dynamic ($\omega^* = 0.56$).

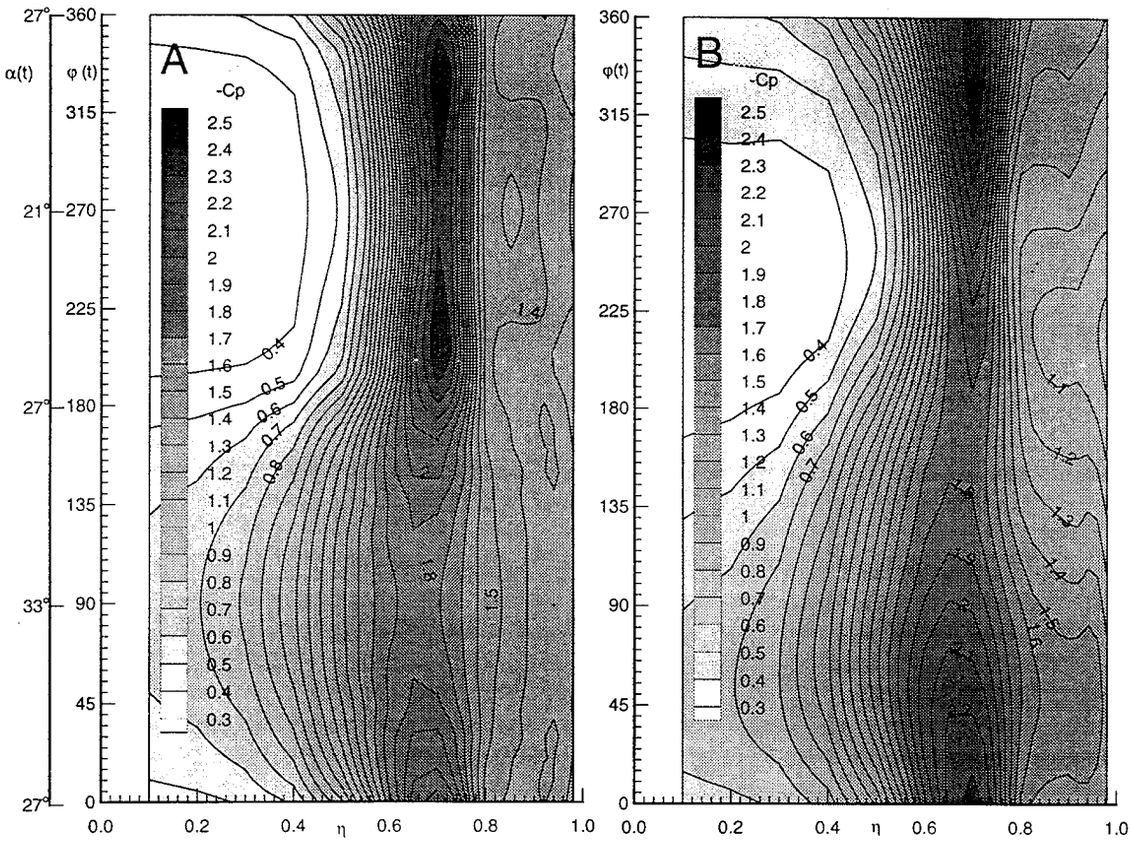

Fig. 8: Quasistatic and dynamic pressure distribution with lines C_p = const. in the section $\xi = 0.6$ for pitching oscillation with $\alpha_0 = 27^o$, $\Delta\alpha = 6^o$, at $Re_\infty = 3.1 * 10^6$. A: quasistatic ($\omega^* = 0$), B: dynamic ($\omega^* = 0.56$).

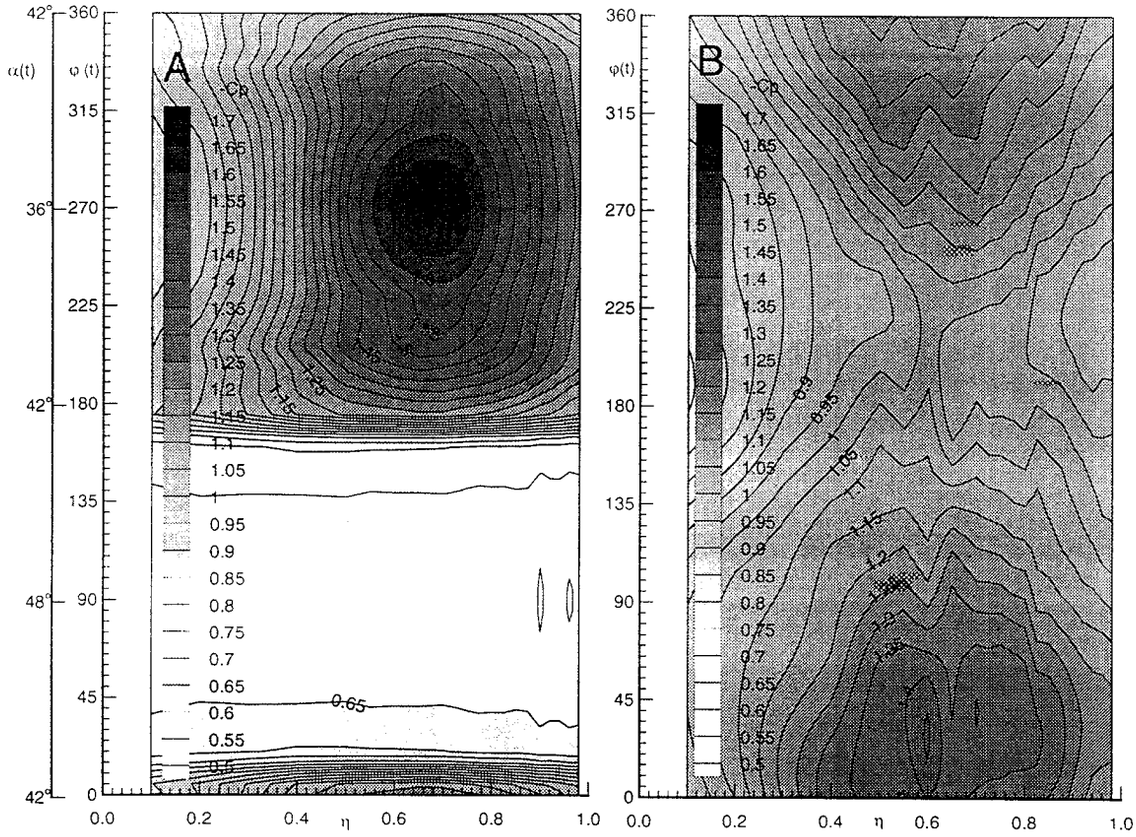

Fig. 9: Quasistatic and dynamic pressure distribution with lines C_p = const. in the section $\xi = 0.6$ for pitching oscillation $\alpha_0 = 42^o$, $\Delta\alpha = 6^o$, $Re_\infty = 3.1 * 10^6$. A: quasistatic ($\omega^* = 0$). B: dynamic ($\omega^* = 0.56$).

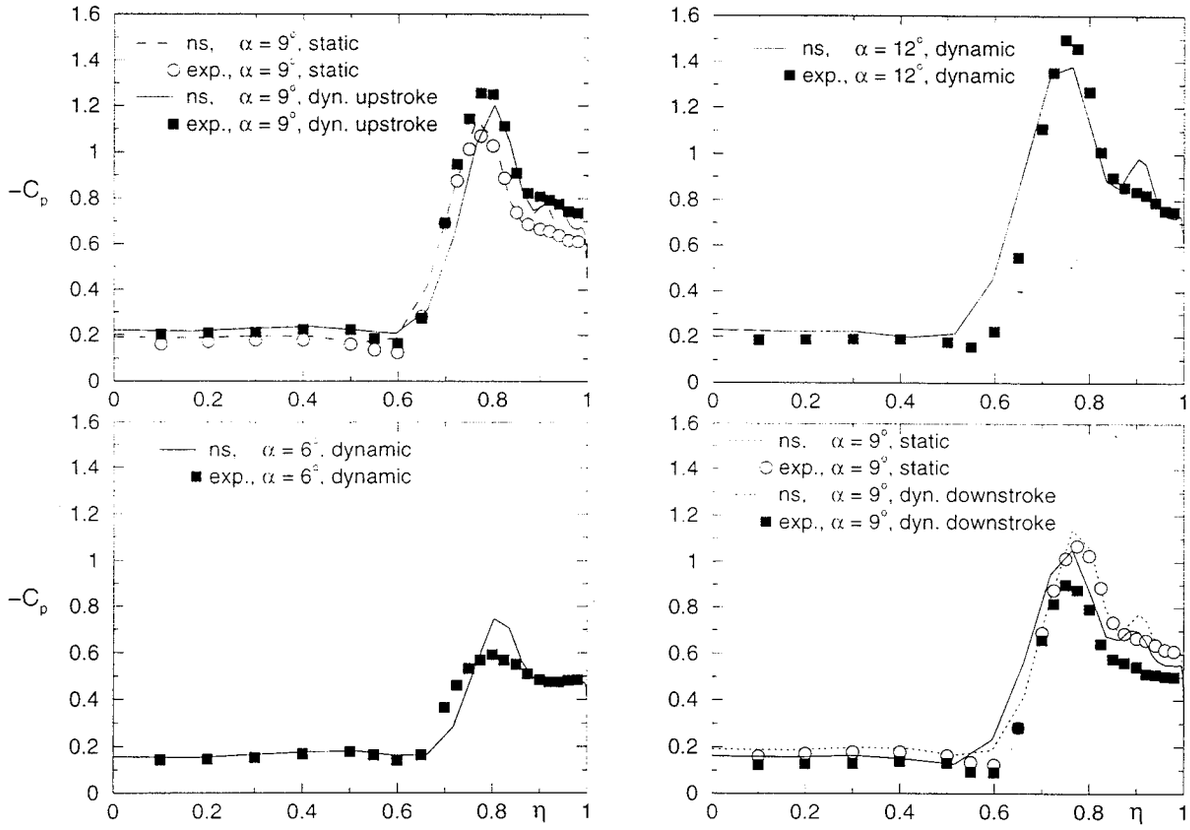

Fig. 10: Comparison of experiment (exp.) and Navier-Stokes calculation (ns). Static and dynamic pressure distributions in the section $\xi = 0.6$ at $Re_\infty = 3.1 * 10^6$. Dynamic parameters: $\alpha_0 = 9^o$, $\Delta\alpha = 3^o$, $\omega^* = 0.56$.